Real-Time Raman Spectroscopic Measurement of Crystallization Kinetics and Its Effect on the Morphology and Properties of Polyolefin Blown Films

Srinivas S. Cherukupalli, Sarah E. Gottlieb, Amod A. Ogale

Department of Chemical Engineering and Center for Advanced Engineering Fibers and Films, Clemson University, Clemson SC 29634-0909

Received 6 July 2004; accepted 15 February 2005
DOI 10.1002/app.22357
Published online in Wiley InterScience (www.interscience.wiley.com).

ABSTRACT: The nonisothermal crystallization half-time ($t_{0.5}$), defined as the time taken for a polymer film to reach half of its equilibrium crystallinity, was estimated from Raman spectroscopic measurements of crystallinity during blown film extrusion of a linear low-density polyethylene (LLDPE) and an isotactic polypropylene (i-PP). The crystalline a- and c-axis orientation of LLDPE and i-PP films, respectively, increased with decreasing crystallization half-time. The transverse direction tensile modulus and tear strengths for LLDPE films also increased with decreasing half-time. However, for i-PP films, only the transverse direction tear strength increased with decreasing $t_{0.5}$, while the machine direction properties did not show a significant dependence on half-time. Our real-time Raman spectroscopy studies provide experimental evidence to theories proposed in the literature[1–3] with regards to the influence of the nonisothermal crystallization process (along the film axis) on the imparted final film structure. © 2005 Wiley Periodicals, Inc. J Appl Polym Sci 98: 1740–1747, 2005

Key words: blown film; isotactic polypropylene; linear low-density polyethylene; online Raman spectroscopy; processing-structure-property relationships

INTRODUCTION

During a film blowing process, the polymer resin molecular characteristics couple with processing conditions to produce the film morphology that ultimately determines the end-use properties. Therefore, a systematic understanding of the microstructure evolution along the film line is essential not only for validation of process model predictions but also for the formulation of processing-structure-property (PSP) relationships to aid in process control/optimization.

Nagasawa et al.[1] reported online measurements of orientation development in blown film extrusion by using the birefringence technique for high-density polyethylene, polybutene-1, and nylon 6. Similar studies on different polyolefins were conducted recently by Ghaneh-Fard et al.[2] and Ito et al.[3] The real-time birefringence experiments[1–3] concluded that the final film orientation is not completely developed by the flow-induced stresses and strain rates near the FLH, but rather, it is the crystallization process of an oriented melt that leads to the observed molecular orientation in the product films. Therefore, the real-time measurements of crystalline phase development along the film line are important for an understanding of the blown film process.

A number of studies have reported the crystallization phenomenon in a fiber spinning process through online experiments.[4–7] But reports on the blown film extrusion have been rather limited. Recent real-time studies of crystallinity have been conducted by Bullwinkel et al.[8] using simultaneous small angle light scattering (SALS) and infrared temperature measurements during film extrusion of an LLDPE. Cakmak et al.[9] developed a noncontact technique for measurement of crystallization in an LDPE film using Raman spectroscopy, light depolarization, and temperature measurements. In our recent work,[10] we have successfully used the online Raman spectroscopic technique to monitor the crystallization process for different processing conditions during film blowing of a linear low-density polyethylene. The rate of crystallization can further be deduced from such crystallinity profiles to determine the structural development along the film line.

Ziabicki[11] proposed that nonisothermal crystallization kinetics can be expressed in terms of the crystallization half-time ($t_{0.5}$), defined as the time taken for a polymer to reach half of its equilibrium crystallinity. The reciprocal of $t_{0.5}$ is proportional to the overall rate of the crystalline phase development. Studies by Dees and Spruiell[4] and Kanai and White[12] have also used the $t_{0.5}$ parameter to explain the nonisothermal crys-

Correspondence to: A. Ogale (ogale@clemson.edu).

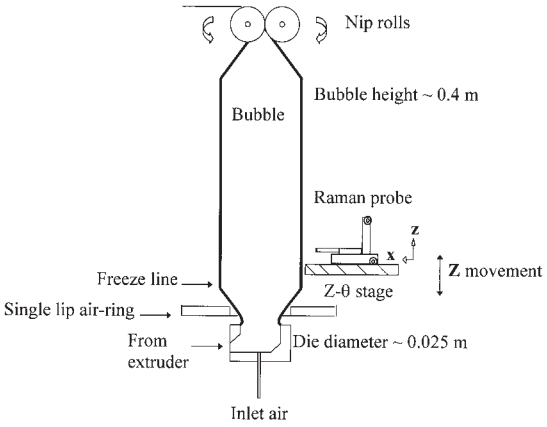

Figure 1 Schematic of the blown film equipment used for online Raman spectroscopy experiments.

tallization rates in melt spinning and blown film extrusion processes, respectively. Other parameters, such as continuous cooling transformation curves,[13,14] crystallization rate parameter,[15] and crystallization rate coefficient,[16] have been reported; a detailed review on nonisothermal crystallization of different polymer systems is also available in the literature.[17]

The primary objective of the present study is to measure nonisothermal crystallization half-times by real-time Raman spectroscopy, and to relate this processing variable to the resulting microstructure and mechanical properties of LLDPE and i-PP blown films.

EXPERIMENTAL

Materials and processing

Two different polyolefin resins were used in this study: (i) a linear low-density polyethylene, Dowlex 2045 (density = 0.92 g/cc); and (ii) an isotactic polypropylene, Dow INSPiRE 112 (density = 0.90 g/cc). Blown films were fabricated using a lab-scale 19 mm, 24 : 1 L/D ratio Haake blown film extruder equipped with a die of 25.4 mm diameter and 0.25 mm gap, and a single-lip air ring. A die temperature of 190°C and 230°C was maintained for LLDPE and i-PP extrusion, respectively, with a polymer mass flow rate of approximately 11.5 g/min for all the experiments. Figure 1 shows a schematic of the equipment setup. The take-up ratio (TUR), blow-up ratio (BUR), and freeze line height (FLH) were treated as the experimental variables; Table I summarizes the processing conditions applied.

Process/Structure measurements

The axial film velocity and diameter profiles were calculated using the video camera tracer technique and from image analysis of the captured bubble pictures, respectively.[18] Online Raman spectra were recorded on a Renishaw System 100 (Gloucestershire, UK) using a near infrared 780 nm-diode laser coupled to an Inphotonics RamanProbe™. Further details on the spectral data acquisition and analysis are reported elsewhere.[10]

TABLE I
Experimental Conditions for Film Processing and Their Corresponding Estimated Crystallization Half-Time Values

Linear low-density polyethylene					
Condition	TUR	BUR	FLH (m)	e_1 (e_2)	$t_{0.5}$
1	3.8	0.4	0.030	2.7 (−2.0)	10.3 ± 1.5
2	3.8	1.5	0.030	2.5 (0.5)	3.8 ± 0.4
3	3.8	2.0	0.027	3.3 (0.9)	3.0 ± 0.3
4	3.8	1.9	0.057	2.2 (0.6)	3.6 ± 0.5
5	11.5	1.5	0.032	7.6 (2.5)	1.0 ± 0.2
6	11.5	1.9	0.060	6.4 (1.5)	2.0 ± 0.3
7	19.0	0.3	0.030	6.1 (−2.6)	4.0 ± 0.5
8	19.0	1.5	0.032	16.7 (3.0)	0.9 ± 0.1
9	19.0	1.9	0.057	10.5 (3.0)	1.8 ± 0.3
Isotactic polypropylene					
Condition	TUR	BUR	FLH (m)	e_1 (e_2)	$t_{0.5}$
1	3.8	1.6	0.025	3.3 (0.8)	1.9 ± 0.3
2	3.8	1.9	0.050	1.7 (0.5)	2.7 ± 0.4
3	11.5	1.6	0.027	10.5 (2.4)	0.75 ± 0.1
4	11.5	2.0	0.055	5.7 (1.0)	1.7 ± 0.3
5	19.0	0.3	0.025	6.1 (−2.3)	2.6 ± 0.4
6	19.0	1.6	0.027	22.8 (2.7)	0.6 ± 0.1
7	19.0	2.0	0.055	10.7 (2.6)	1.1 ± 0.2

TUR = take-up ratio, BUR = blow-up ratio, FLH = freeze line height, e_1 = machine direction strain rate, e_2 = transverse direction strain rate, $t_{0.5}$ = crystallization half-time.

The crystallinity of final films was measured using the established offline techniques of differential scanning calorimetry (DSC) and wide-angle X-ray diffraction (WAXD). Enthalpies of fusion (ΔH_f) of the film samples were obtained from a Perkin–Elmer Pyris 1 DSC instrument. Crystallinity was subsequently estimated from ΔH_f by using a value of 60 cal g^{-1} and 35 cal g^{-1} for the enthalpy of fusion of perfectly crystalline LLDPE[19] and i-PP,[20] respectively. Wide-angle X-ray diffraction patterns were obtained from a Rigaku 2-D diffractometer (Rigaku/MSC) using Cu-Kα radiation with conditions of 40 KV and 30 μA. All of the WAXD data were taken in transmission mode with the films stacked to obtain a constant thickness of approximately 100 μm. The collected patterns were then analyzed using POLAR® and GRAMS 3D® software to refine the crystalline peaks from the amorphous halo. An equilibrium crystallinity of about 40% for LLDPE and 54% for i-PP was obtained for all the samples.

Crystalline orientation was quantified along different crystallographic axes using Hermans' orientation factor for a uniaxial symmetry:[4]

$$f = 0.5(3\langle\cos^2\varphi\rangle - 1) \quad (1)$$

where $<\cos^2\varphi>$ is the average value of the cosine squared of the angle φ between the film machine direction and a crystallographic axis. According to eq. (1), the orientation factor is zero for a random orientation, and 1.0 and -0.5 for a perfectly oriented sample parallel and perpendicular to the reference axis, respectively. For LLDPE, $<\cos^2\varphi>$ values from the azimuthal intensity distributions of (200) and (020) yielded the values of f_a and f_b, respectively. For the polyethylene orthorhombic cell, the value of f_c could be obtained using the equation:

$$f_a + f_b + f_c = 0 \quad (2)$$

For isotactic polypropylene, the method of Wilchinsky[21,22] was used to compute f_c:

$$\langle\cos^2\Phi_c\rangle = 1 - 1.099\langle\cos^2\Phi_{110}\rangle - 0.901\langle\cos^2\Phi_{040}\rangle \quad (3)$$

The values of $<\cos^2\Phi_{110}>$ and $<\cos^2\Phi_{040}>$ were obtained from azimuthal intensity measurements on the (110) and (040) reflections, respectively. The value of f_b can be computed from the intensity distribution in the (040) reflection; while $f_{a'}$, describing the orientation of a nonprincipal crystallographic axis (a') defined perpendicular to the b- and c-axes, can be estimated using eq. (2) (with $f_{a'}$ substituted for f_a). The principal a-axis for i-PP monoclinic crystal makes an angle of 99.3° to the c-axis.

Mechanical properties

Tensile properties along the machine and transverse directions of the films were measured using a Satec tensile tester (Model 10,000, Canton, MA) as per ASTM D882 procedure. The gauge length and width of the samples were nominally 50 mm × 12.5 mm for MD, and 25 mm × 12.5 mm for TD measurements. The Elmendorf tear strength was measured in accordance with ASTM D-1922 with rectangular samples of 63 mm × 76 mm; the direction of tear was along the longer dimension (76 mm). The film thickness was measured using a Nikon Digimicro (Model MFC-101, Melville, NY).

RESULTS AND DISCUSSION

Real-Time crystallization kinetics

Representative online Raman spectra along the machine direction (axial distance) of the blown film are displayed in Figures 2(a) and 2(b) for LLDPE and i-PP, respectively. The results show that as the polymer travels from a location below the freeze line to that above, the characteristic crystalline peak intensities at 1418 cm^{-1} [LLDPE, Fig. 2(a)] and 809 cm^{-1} [i-PP, Fig. 2(b)] steadily increase as a consequence of the crystallization process.[23–26]

The crystalline phase content at different positions along the axial distance can then be determined from the Raman spectra. For linear low-density polyethylene, the ratio of 1418 cm^{-1} peak intensity to the combined intensities of 1295 cm^{-1} and 1305 cm^{-1} peaks were used to estimate crystallinity[23,24]; the details for crystallinity calculations have been described in our previous study.[10] For isotactic polypropylene, Nielsen et al.[26] reported that intensities (I_j) in the spectral region from 809–841 cm^{-1} can be analyzed to obtain the crystalline fraction (X_c):

$$X_c = I_{809}/(I_{809} + I_{830} + I_{841}) \quad (4)$$

It is noted that the 830 cm^{-1} peak was very weak in all of our measured spectra and did not contribute significantly in the present calculations. The final film crystallinity values calculated from Raman spectroscopy were found to be approximately 10% higher than those obtained from WAXD results.

Figures 3(a) and 3(b) present the crystallinity profiles for representative conditions during film blowing of LLDPE and i-PP, respectively. As expected, the data suggest that the crystallization process starts as the extrudate reaches the FLH, increases

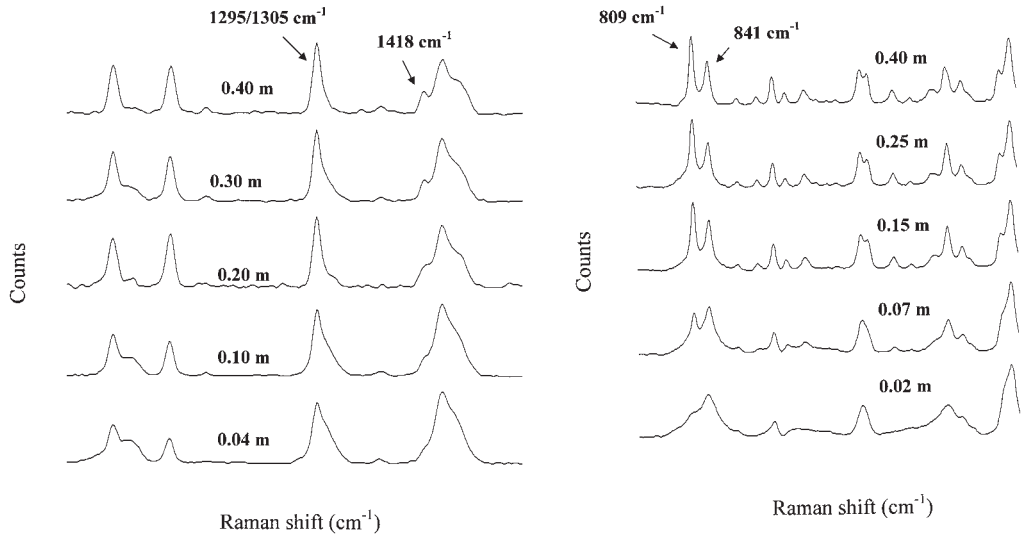

Figure 2 (a) Raman spectra for linear low-density polyethylene in the range of 1000–1500 cm^{-1} along the axial distance of the blown film line. TUR = 3.8, BUR = 1.5, FLH = 0.03 m. (b) Raman spectra for isotactic polypropylene in the range of 700–1450 cm^{-1} along the axial distance of the blown film line. TUR = 3.8, BUR = 1.6, FLH = 0.025 m.

along the film line, and finally plateaus. The nonisothermal crystallization half-time can then be estimated from the crystallinity profiles as plotted in Figures 3(a) and 3(b). A $t_{0.5}$ of 3.8 s and 1.9 s were obtained for LLDPE and i-PP, respectively. It is noted that the absolute $t_{0.5}$ values between the different polymers are not comparable.

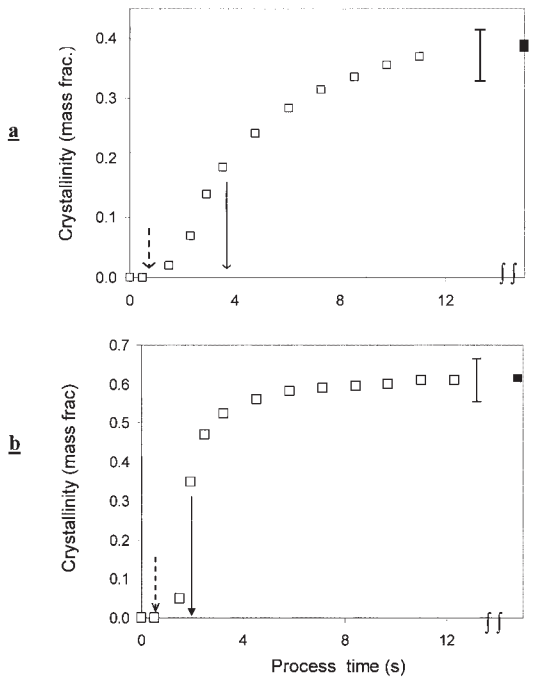

Figure 3 Crystallinity profiles for (a) LLDPE and (b) I-PP at TUR of 3.8 and BUR of ~ 1.5. Solid symbols represent data collected after the film had attained equilibrium crystallinity levels (t ~ 24 hrs). Dotted arrows indicate the nominal process time at which the freeze line height is reached; solid arrows indicate the crystallization half-time.

The measured crystallization half-times for the various conditions during film extrusion of LLDPE and i-PP are summarized in Table I. With an increase in TUR from 3.8 and 11.5 (Conditions: 2, 5 for LLDPE; 1, 3 for i-PP), the crystallization half-time decreases from 3.8 s to 1.0 s for LLDPE, and from 1.9 s to 0.75 s for i-PP, indicating a significant increase in the rate of crystallization. This dramatic increase in the crystallization rate is likely a result of increased bubble cooling rates due to the thinning of film, and increased stresses acting on the bubble as a consequence of higher take-up ratio.

If strain rates are indicative of the stresses acting on the film, then the machine and transverse direction strain rates (e_1 and e_2, respectively) presented in Table I show an increase in applied stresses with an increase in TUR. As the TUR is increased, the stresses acting on the film cause the polymer molecules to align preferentially along the flow direction and increase the rate of crystallization. Thus, for a given resin, a higher rate was observed at a TUR of 11.5 as compared to a TUR of 3.8. The concept of flow-induced crystallization (FIC) has been discussed in the literature.[27] However, a further change in TUR from 11.5 to 19.0 (Conditions 5, 8 for LLDPE; 3, 6 for i-PP; Table I) does not change the half-time values, indicating a probable saturation of the FIC effect.[4]

The decrease in crystallization half-time with increasing BUR (Conditions: 1–3 for LLDPE; 5, 6 for i-PP; Table I) may also have some basis in the FIC theory; the strain rate data are as presented in Table I. However, for different FLHs (Conditions 3, 4 for LL-

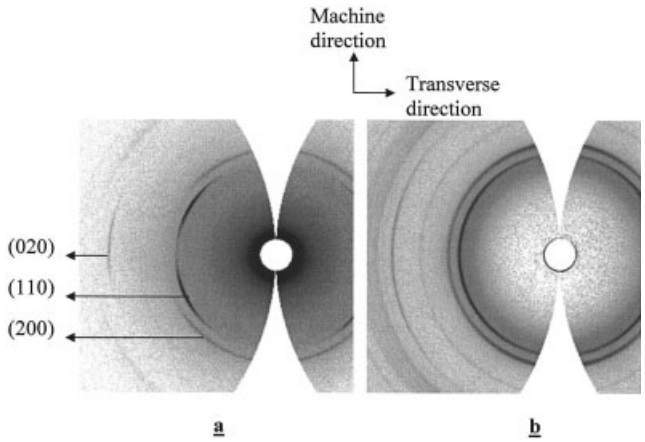

Figure 4 Wide angle X-ray diffractograms for linear low-density polyethylene blown films for two different crystallization half-times: (a) 1.0 s and (b) 10.3 s.

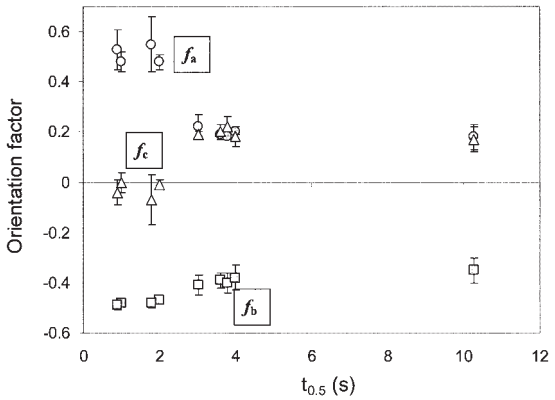

Figure 5 Orientation factors ($f_{a,b,c}$) for linear low-density polyethylene blown films plotted as a function of crystallization half-time for different processing conditions.

DPE; Table I), the $t_{0.5}$ values did not show significant differences, likely due to small differences in the external bubble cooling conditions that could be realized in this study.

Crystalline orientation—real-time crystallization kinetics

Linear low-density polyethylene

Wide angle X-ray diffractograms for LLDPE blown films for two limiting crystallization half-times are shown in Figures 4(a) and 4(b). The scattering from the (110), (200), and (020) planes are identified on the figures. For the different processing conditions, the b-axis (identified by the (020) plane) has a scattering intensity predominantly along the equator, indicating an orientation in the direction perpendicular to the reference machine direction. On the other hand, the intensity distribution of the (200) plane changed markedly with $t_{0.5}$, showing that the a-axis is preferentially oriented along the machine direction with decreasing $t_{0.5}$ values.

The crystalline orientation factors ($f_{a,b,c}$) computed from the WAXD data are plotted in Figure 5 as a function of crystallization $t_{0.5}$ for different processing conditions. It can be observed that the f_a values remain constant until a $t_{0.5}$ of 3 s and then increase rapidly with decreasing $t_{0.5}$, indicating a tendency of the a-axis to be oriented along the machine direction with increasing rate of crystallization. In contrast, f_c decreases close to zero, signifying a random orientation of the chain axis. The values for f_b gradually approach -0.5 with decreasing $t_{0.5}$, representing an orientation increasingly perpendicular to the machine direction.

Isotactic polypropylene

Figures 6(a) and 6(b) present the wide angle X-ray diffractograms of i-PP films processed at limiting crystallization half-times (Table I). The (040) and (110) monoclinic reflections that were used to calculate Herman's crystalline orientation factors according to Wilchinsky's method are identified in the figure. The diffractograms also show the typical bimodal distribution of the (110) reflection, consisting of equatorial and meridional components with respect to the reference direction. A detailed discussion of bimodal crystal orientation distribution in i-PP has been provided by Clark and Spruiell.[28]

Figure 7 displays Hermans' crystalline orientation factors ($f_{a'/b/c}$) for i-PP films plotted as a function of crystallization half-time values at different processing conditions. It was observed that the c-axis orientation (f_c) increases with increasing crystallization rate (i.e., decreasing $t_{0.5}$) and the chain axes progressively align with the machine direction. The f_b values remain unchanged at approximately -0.5, indicating a near-perpendicular alignment of the b-axes with respect to the reference direction for all the films. On the other

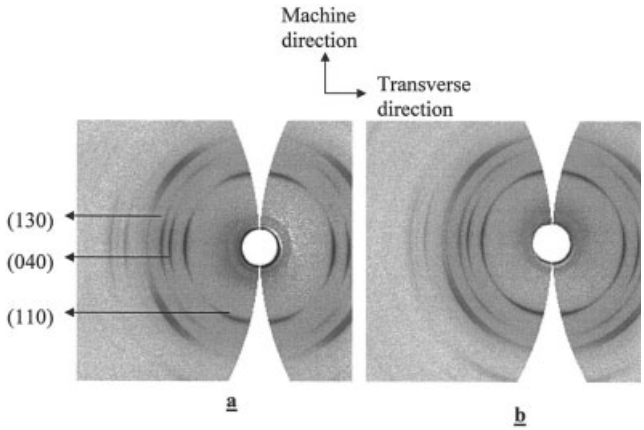

Figure 6 Wide angle X-ray diffractograms for isotactic polypropylene blown films at two different crystallization half-times: (a) 0.6 s and (b) 2.7 s.

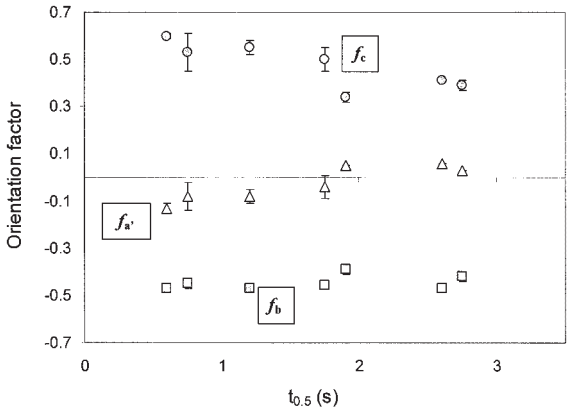

Figure 7 Orientation factors ($f_{a,b,c}$) for isotactic polypropylene blown films plotted as a function of crystallization half-time for different processing conditions.

hand, $f_{a'}$ remains close to zero, representing a random orientation of the chain axis.

Effect of crystallization half-time on the tensile and tear properties

Figures 8(a) and 8(b) display the LLDPE and i-PP tensile moduli as a function of the crystallization half-times for different processing conditions. For LLDPE, the MD values showed a relative insensitivity to half-times, but the TD modulus increases with decreasing $t_{0.5}$. On the other hand, the MD and TD moduli for i-PP did not show any significant dependence on $t_{0.5}$.

The above result is consistent with composite theories for morphology-property relationships of polyolefin films.[29,30] The film can be considered as a composite with a "hard" crystalline phase and a "soft" noncrystalline phase stacked along the machine direction. For deformations along the MD, both phases are stretched in series and the modulus is dominated by that of the "soft" component. For deformations along the TD, the crystalline and noncrystalline phases are stretched in parallel and the stresses are distributed primarily along the long axis (b-axis) of the rigid crystalline lamellae. Thus, with increasing orientation of the load-bearing lamellae along the TD ($f_b \rightarrow -0.5$), the transverse direction modulus increases. As shown in Figure 5, the lamellar growth axis for LLDPE films progressively orients along the transverse direction for lower half-time values (i.e., high crystallization rate), resulting in higher tensile modulus values as observed in Figure 8(a). However for i-PP films, the f_b values are nearly equal to -0.5 for the different processing conditions (Fig. 7), resulting in approximately constant TD moduli.

Figures 9(a) and 9(b) present the tear strengths for LLDPE and i-PP blown films, respectively, as a func-

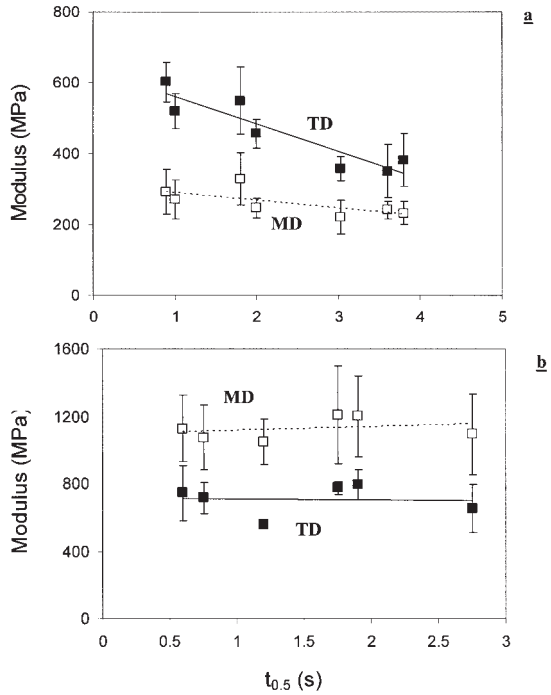

Figure 8 Tensile modulus along the machine and transverse directions plotted as a function of crystallization half-times for different processing conditions: (a) linear low-density polyethylene, and (b) isotactic polypropylene. Solid and dashed lines indicate linear least-squared fits to the transverse and machine direction data, respectively.

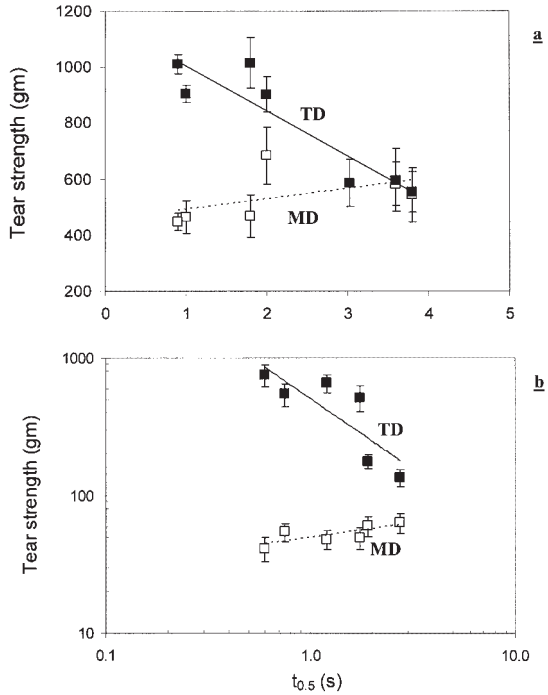

Figure 9 Tear strength along the machine and transverse directions plotted as a function of crystallization half-times for different processing conditions: (a) linear low-density polyethylene, and (b) isotactic polypropylene. Solid and dashed lines indicate linear least-squared fits to the transverse and machine direction data, respectively.

tion of crystallization half-time. For LLDPE, a low value of $t_{0.5}$ corresponded to low MD and high TD tear strengths. On the other hand, Figure 9b indicates that the MD tear strength values of i-PP films are relatively low and moderately insensitive to $t_{0.5}$ values, whereas the TD tear strength decreases with crystallization half-time.

The tear strength correlations in Figures 9a and 9b can be explained on the basis of crack propagation during a tear process through the weakest regions, that is, the noncrystalline region.[31–34] Previous studies on LLDPE[31,32] and PP[33,34] films have established that with increasing directional orientation, the noncrystalline chains also preferentially align along the same direction. Consequently, if more noncrystalline chains are oriented along the MD, the tear crack would propagate more easily along the MD, thus decreasing the MD tear strength. In contrast, the increased orientation of the noncrystalline chains along the MD translates into higher resistance for tear propagation along the TD. Therefore, as the crystalline a-axis for LLDPE and c-axis for PP become more oriented towards the MD (Figs. 5 and 7) with decreasing $t_{0.5}$, the TD tear strength increases.

Literature studies on polyolefin blown films have used stress (or strain rate) at the freeze line height as the processing parameter that controls the film morphology and, therefore, properties.[35–38] However, real-time birefringence measurements on different polyolefins have concluded that the molecular orientation primarily develops during the crystallization process, which takes place past the FLH.[1–3] In other words, the observed final film morphology is likely due to consolidation of the initial chain orientation (caused by applied stresses) through the nonisothermal crystallization process.[39] Crystallization half-time was considered in this study as a relevant parameter to describe the nonisothermal crystallization process along the blown film line and was estimated in real-time using Raman spectroscopy. The obtained half-time values for LLDPE and i-PP films related well with the tensile and tear properties. From a practical standpoint, such relationships based on online measurements can be applied to optimize and control the blown film process. The real-time measurements at various positions along the film line can be used in conjunction with a multivariate calibration technique to directly predict the final film properties.

CONCLUSIONS

The relationship between crystallization half-time (estimated using real-time Raman spectroscopy), the final film morphology, and properties of linear low-density polyethylene and isotactic polypropylene films was investigated. For the range of processing conditions studied, the results indicated that the a- and c-axis crystalline orientation for LLDPE and i-PP films, respectively, increased with decreasing crystallization half-time (i.e., increasing crystallization rate). The transverse tensile modulus and tear strengths for LLDPE films also increased with decreasing half-time. However, for i-PP films, only the transverse direction tear strength increased with decreasing $t_{0.5}$, while the machine direction properties did not show a significant dependence on half-time. Such correlations, based on real-time measurements of microstructure, offer an opportunity for better process control and optimization during a film blowing process.

This work was supported by the Engineering Research Centers Program of the National Science Foundation under NSF Award Number EEC-9731680. Any opinions, findings, conclusions, or recommendations expressed in this material are those of the authors and do not necessarily reflect those of the National Science Foundation. We thank Mr. Tom Butler and Dr. R. Patel for useful discussions.

References

1. Nagasawa, T.; Matsumura, T.; Hoshino, S. Appl Polym Symp 1973, 20, 275.
2. Ghaneh-Fard, A.; Carreau, P. J.; Lafleur, P. G. Int Polym Proc 1997, 12, 136.
3. Ito, H.; Suzuki, K.-I.; Kikutani, T.; Kang, H.-J.; Kanai, T. SPE ANTEC Tech Papers 2004, 50, 1856.
4. Dees, J.; Spruiell, J. J Appl Polym Sci 1974, 18, 1053.
5. Abbott, L.; White, J. Appl Polym Symp 1973, 20, 247.
6. Nakamura, K.; Watanabe, T.; Katayama, K.; Amano, T. J Appl Polym Sci 1972, 16, 1077.
7. Paradkar, R.; Sakhalkar, S.; He, X.; Ellison, M. J Appl Polym Sci 2003, 88, 545.
8. Bullwinkel, M.; Campbell, G.; Rasmussen, D.; Krexa, J.; Brancewitz, C. Int Polym Proc 2001, 16, 39.
9. Cakmak, M.; Serhatkulu, F.; Graves, M.; Galay, J. SPE ANTEC Tech Papers 1997, 43, 1794.
10. Cherukupalli, S.; Ogale, A. A. Polym Eng Sci 2004, 44, 1484.
11. Ziabicki, A. Appl Polym Symp 1967, 6, 1.
12. Kanai, T.; White, J. Polym Eng Sci 1986, 24, 1185.
13. Spruiell, J.; White, J. Polym Eng Sci 1975, 15, 660.
14. Spruiell, J. Structure Development During Polymer Processing; Kluwer Academic Publishers: Dordrecht, 2000; p 195.
15. Khanna, P. Polym Eng Sci 1990, 30, 1615.
16. Zhang, R.; Zheng, H.; Lou, X.; Ma, D. J Appl Polym Sci 1994, 51, 51.
17. Di Lorenzo, M.; Silvestre, C. Prog Polym Sci 1999, 24, 917.
18. Huang, T.; Campbell, G. Adv Polym Tech 1985, 5, 181.
19. Mirabella, F.; Bafna, A. J Polym Sci Part B: Polym Phys 2002, 40, 1637.
20. Monasse, B.; Haudin, J. M. Colloid Polym Sci 1985, 263, 822.
21. Alexander, L. E. X-Ray Diffraction Methods in Polymer Science; John Wiley & Sons, Inc: New York, 1969; p 247.
22. Nadella, H.; Henson, H.; Spruiell, J.; White, J. J Appl Polym Sci 1977, 21, 3003.
23. Strobl, G. R.; Hagedorn, W. J Polym Sci Polym Phys Ed 1978, 16, 1181.
24. Clas, S.-D.; Heyding, R.; McFaddin, D.; Russell, K.; Scamell-Bullock, M. J Polym Sci Part B: Polym Phys 1988, 26, 1271.
25. Fraser, G.; Hendra, P.; Watson, D.; Gall, M.; Willis, H.; Cudby, M. Spectrochim Acta 1972, 29A, 1525.

26. Nielsen, A.; Batchelder, D.; Pyrz, R. Polymer 2002, 43, 2671.
27. Doufas, A.; McHugh, A. J Rheol 2001, 45, 1085.
28. Clark, E.; Spruiell, J. Polym Eng Sci 1976, 16, 176.
29. Zhou, H.; Wilkes, G. J Mater Sci 1998, 33, 287.
30. Krishnaswamy, R. K.; Lamborn, M. J. Polym Eng Sci 2000, 40, 2385.
31. Chen, H.; Chau, C.; Butler, T.; Landes, B.; Bishop, M.; Bellmore, D.; Chum, S.; Dryzga, C. SPE ANTEC Tech Papers 2003, 49, 1401.
32. Krishnaswamy, R.; Sukhadia, A. Polymer 2000, 41, 9205.
33. Yuksekkalayci, C.; Yilmazer, U.; Orbey, N. Polym Eng Sci 1999, 39, 1216.
34. Umemura, T.; Akiyama, K. IEEE T Electr Insul 1986, EI–21, 137.
35. Tas, P. Ph.D. Dissertation, University of Eindhoven, 1994.
36. Babel, A.; Campbell, G. Tappi J 1995, 78, 199.
37. Choi, K.-J.; Spruiell, J.; White, J. J Polym Sci Polym Phys Ed 1982, 20, 27.
38. Kwack, T.; Han, C. J Appl Polym Sci 1988, 35, 363.
39. Keller, A.; Kolnaar, J. Prog Colloid Polym Sci 1993, 2085, 50.